

Modelling Brittle Fracture Propagation in Gas and Dense-phase CO₂ Transportation Pipelines

Haroun Mahgerefteh*, Peng Zhang and Solomon Brown
Department of Chemical Engineering, University College London
Torrington place, London WC1E 7 JE

Abstract

The development and application of a fluid-structure interaction model for simulating the transition of a through-wall defect in pressurised dense (150 bar, 283.15 K) and gas phase (34 bar, 283.15 K) CO₂ pipelines into a running brittle fracture is presented. Given the economic incentives, the fracture model is employed to test the suitability of the existing stock of natural gas pipelines with the relatively high ductile to brittle transition temperatures of 0 °C and -10 °C for transporting CO₂ in the terms of their resistance to brittle fracture propagation. The hypothetical but nevertheless realistic scenarios simulated involve both buried and above ground 10 km long, 0.6 m i.d pipelines. Based on the assumption of no blowout of the surrounding soil upon the formation of the initial leak, the results show that the transition of the leak into a running brittle fracture in buried CO₂ pipelines is far more likely as compared to above ground pipelines. In addition, gas phase pipelines are more prone to undergoing a propagating brittle fracture as compared to dense phase pipelines despite the lower operating pressures of the former. Furthermore, counter-intuitively, isolation of the feed flow following the discovery of a leak is shown to facilitate brittle fracture failure. The initial defect geometry on the other hand is shown to have a profound impact on the pipeline's resistance to propagating brittle fractures.

Key words: CO₂ pipelines; brittle fracture; stress-induced failure; depressurisation; safety; risk assessment

*Corresponding author: h.mahgerefteh@ucl.ac.uk

1. Introduction

As the planning for Carbon Capture and Sequestration (CCS) proceeds, the use of long distance networks of pressurised pipelines for the transportation of the captured CO₂ for subsequent sequestration is becoming inevitable. Given that CO₂ is considered to be toxic at concentrations higher than 7% (Harper et al., 2011), the

safety of CO₂ pipelines is of paramount importance and indeed pivotal to the public acceptability of CCS as a viable means for tackling the impact of global warming.

It is noteworthy that CO₂ pipelines have been in operation in the US for over 30 year for enhanced oil recovery (Bilio et al., 2009; Seevam et al., 2008); however, these are confined to low populated areas. Additionally, given their small number, it is not possible to draw a meaningful statistical representation of the overall risk. Parfomak and Fogler (2007) propose that ‘statistically, the number of incidents involving CO₂ pipelines should be similar to those for natural gas transmission pipelines’.

Clearly, given the heightened public awareness in environmental issues, even a single incident involving the large-scale escape of CO₂ near a populated area may have an adverse impact on the introduction of the CCS technology.

Propagating or running fractures are considered as the most catastrophic type of pipeline failure given that they result in a massive escape of inventory in a short space of time. As such it is highly desirable to design pipelines with sufficiently high fracture toughness such that when a defect reaches a critical size, the result is a leak rather than a long running fracture. In the case of CO₂ pipelines such types of failure will be of particular concern in Europe as large pipeline sections will inevitably be onshore, some passing near or through populated areas (Serpa et al., 2011). In addition, there is significant financial incentive in using the existing stock of hydrocarbon pipelines for transporting CO₂ (Serpa et al., 2011). Given the very different properties of CO₂ as compared to hydrocarbons, all safety issues regarding fluid/pipeline compatibility must be addressed *a priori*.

A fracture may propagate in either a ductile or a brittle mode. However, there are subtle, yet important differences in the respective propagation mechanisms worthy of discussion. Ductile fractures, characterised by the plastic deformation of the pipeline along the tear are the more common of the two modes of failure and therefore best understood. These may commence following an initial tear or a puncture in the pipeline, for example due to third party damage or corrosion. The potential for this initial through-wall defect transforming into a propagating ductile fracture may be assessed using the simple well-established Battelle Two Curve (BTC) methodology

(Maxey, 1974). In essence the above involves the comparison of the pipeline decompression and the crack tip velocity curves. The crack will propagate as long as the decompression wave speed in the fluid is slower than the crack tip velocity. The BTC approach was recently extended by the present authors (Mahgerefteh et al., 2011) based on the coupling the fluid decompression and the crack velocity curves. This enabled the prediction of the variation of the crack length with time and hence the crack arrest length. Given the almost instantaneous transformation of the initial tear into a ductile fracture running at high velocity (ca. 200-300 m/s), heat transfer effects between the escaping fluid and the pipe wall during the propagation process will be insignificant. As such the transient pressure stress is the only driving force for propagating a ductile fracture.

The propagation mechanism in the case of brittle fractures is somewhat different. A situation may arise in which the pressure inside the pipeline at the time of formation of a puncture or a leak will be insufficient to drive a ductile fracture. However, with the passage of time, the Joule-Thomson expansion induced cooling of the escaping fluid will lower the pipe wall temperature in the proximity of the leak. In the event that the pipe wall temperature reaches its Ductile to Brittle Transition Temperature (DBTT), for most pipeline materials, there will be an almost instantaneous and significant drop in the fracture toughness. In such cases, depending on the initial defect size and geometry, if the prevailing pressure and thermal stresses exceed the critical fracture toughness (Mahgerefteh and Atti, 2006), a running brittle fracture will occur.

As such the modelling of brittle fractures requires the consideration of both the transient thermal and pressure stresses in the proximity of the initial through-wall defect.

Three factors render CO₂ pipelines especially susceptible to brittle fractures as compared to hydrocarbon pipelines (Bilio et al., 2009). These include CO₂'s high saturation pressure and its significant sensitivity to the presence of even small amounts of impurities (Mahgerefteh et al., 2012), its 'slow' depressurisation

following a leak especially during the liquid/gas phase transition and finally its high Joule-Thomson expansion induced cooling.

Although brittle fracture propagation in CO₂ pipelines has been raised as an issue of possible concern (Andrews et al., 2010), to date, no experimental test data or comprehensive mathematical modelling work on the topic has been reported. This is of especial concern given the economic incentives in using existing natural gas pipelines for transporting CO₂. Such pipelines are more susceptible to brittle fractures as compared to newer pipeline materials given their much higher DBTT (cf. -10 °C with -80 °C). Given the relatively short time frames being proposed for CCS introduction, the development of suitable mathematical models for assessing the susceptibility of CO₂ pipelines to brittle fractures is very timely.

In a previous publication (Mahgerefteh and Atti, 2006), we presented a fluid-structure interaction model for simulating brittle fractures in pressurised pipelines. However, the simulation data reported based on application of the model was limited to hydrocarbon pipeline inventories. Given their very different thermodynamic decompression trajectories, it is impossible to extend the findings to CO₂ pipelines. Additionally, the modelling employed an over-simplified heat transfer mechanism in which the impact of the radial temperature gradient across the pipe wall thickness on the resulting thermal stresses was ignored. Given that the latter is the main mechanism responsible for facilitating a brittle fracture, its accurate determination is important.

In this paper, we present the development and application of a fully coupled fluid-structure interaction model for simulating brittle fracture propagation in gas and dense phase CO₂ pipelines. Given the obvious economic incentives, the simulations using the model mainly focus on testing the suitability of the current stock of natural gas pipelines for transporting CO₂ in terms of their propensity to brittle fracture propagation. The impacts of fluid phase, the pipe wall thickness, Ductile-Brittle-Transition Temperature (DBTT), the crack geometry, feed temperature, stream impurities as well as flow isolation on brittle fracture propagation behaviour are tested.

2. Theory

The development of the brittle fracture model involves the formulation of the following elements:

- i) a fluid dynamics model for predicting the transient fluid temperature and pressure during the decompression process following the initial leak;
- ii) a heat transfer model for predicting the localised cooling of the pipe wall by the escaping CO₂;
- iii) a fracture model for evaluating the resultant pressure and thermal stresses at the defect tip.

2.1 Fluid Dynamics Model

The background theory of the fluid dynamics model employed for predicting the fluid flow parameters including the transient fluid temperature and pressure following pipeline failure has been described elsewhere (Mahgerefteh et al., 2009, 2008; Oke et al., 2003) and hence only a brief account is given here. The governing conservation equations for mass, energy and momentum are respectively given by:

$$\frac{d\rho}{dt} + \rho \frac{\partial u}{\partial x} = 0 \quad (1)$$

$$\rho \frac{\partial u}{\partial t} + \rho u \frac{\partial u}{\partial x} + \frac{\partial P}{\partial x} = \alpha \quad (2)$$

$$\rho \frac{dh}{dt} - \frac{dP}{dt} = q_h - u\beta_x \quad (3)$$

$$\beta_x = -\frac{2f_w \rho u |u|}{D_{in}} \quad (4)$$

where, u , h , ρ and P are the velocity, specific enthalpy, density and pressure of the fluid as function of time, t , and space, x . q_h is the heat transferred through the pipe wall to the fluid and β_x is the friction force term defined in (4), in which D_{in} is pipeline inner diameter and f_w is the Fanning friction factor given by (Chen, 1979):

$$\frac{1}{\sqrt{f_{in}}} = -2 \log \left(\frac{\varepsilon / D_{in}}{3.7065} - \frac{5.0452}{Re} \cdot \log \left(\frac{(\varepsilon / D_{in})^{1.1098}}{2.8257} + \frac{5.8506}{Re^{0.8901}} \right) \right) \quad (5)$$

where ε , and D_{in} are the pipe roughness and internal diameter respectively.

Also

$$\alpha = -(\beta_x + \rho g \sin \theta) \quad (6)$$

where, g and θ are the gravitational acceleration and the angle of inclination of the pipeline to the horizontal respectively.

The above quasi-linear conservation equations are solved numerically using the method of characteristics (Zucrow and Hoffman, 1975). The technique is based on the principle of the propagation of characteristic waves, which handles the choked flow intrinsically via the Mach line characteristics. The modified Peng-Robinson equation of state (Wu and S. Chen, 1997) is employed to obtain the relevant fluid thermodynamic and phase equilibrium data.

2.2 Heat Transfer

2.2.1 Pipe wall temperature

The 3-D heat transfer within the pipe wall is governed by the following heat conduction equation (Cengel, 2003):

$$\rho C \frac{\partial T}{\partial t} + \frac{\partial}{\partial x} \left(\kappa \frac{\partial T}{\partial x} \right) + \frac{\partial}{\partial y} \left(\kappa \frac{\partial T}{\partial y} \right) + \frac{\partial}{\partial z} \left(\kappa \frac{\partial T}{\partial z} \right) = 0 \quad (7)$$

where, κ and C are the thermal conductivity and specific heat respectively. Equation (7) is solved numerically using the finite volume method (Tannehill et al., 1997) by discretising the pipe wall into small elements. The corresponding heat balance for each element is given by:

$$\begin{aligned}
& k_{i-1/2,j,k} \Delta y \Delta z \frac{T_{i-1,j,k} - T_{i,j,k}}{\Delta x} + k_{i,j-1/2,k} \Delta x \Delta z \frac{T_{i,j-1,k} - T_{i,j,k}}{\Delta y} + k_{i,j,k-1/2} \Delta x \Delta y \frac{T_{i,j,k-1} - T_{i,j,k}}{\Delta z} \\
& - k_{i+1/2,j,k} \Delta y \Delta z \frac{T_{i,j,k} - T_{i+1,j,k}}{\Delta x} - k_{i,j+1/2,k} \Delta x \Delta z \frac{T_{i,j,k} - T_{i,j+1,k}}{\Delta y} - k_{i,j,k+1/2} \Delta x \Delta y \frac{T_{i,j,k} - T_{i,j,k+1}}{\Delta z} \\
& = \rho C_{i,j,k} \Delta x \Delta y \Delta z \frac{T_{i,j,k}^{t+\Delta t} - T_{i,j,k}^t}{\Delta t}
\end{aligned} \tag{8}$$

where $k_{i,j,k+1/2}$ are the thermal conductivities between the neighbouring cells (i,j,k) and (i,j,k+1).

Thus, by knowing the temperature of cell (i,j,k) and its six adjacent cells at time, t the temperature of cell (i,j,k) at time $t + \Delta t$ can be calculated.

The time-step, Δt is determined using the following stability criterion (Efring, 1990):

$$\Delta t < \min_{i,j,k} \left(\frac{C_{i,j,k} \Delta x \Delta y \Delta z}{k_{i-1/2,j,k} + k_{i,j-1/2,k} + k_{i,j,k-1/2} + k_{i+1/2,j,k} + k_{i,j+1/2,k} + k_{i,j,k+1/2}} \right) \tag{9}$$

The main modes of heat transfer during pipeline depressurisation are:

- i) ambient air to outer pipe wall heat transfer;
- ii) axial forced convective heat transfer between the escaping fluid and the puncture plane;
- iii) convective heat transfer between the flowing fluid and the inner pipe wall.

2.2.2 Ambient to outer pipe wall heat transfer

The heat transfer coefficient between the pipe wall and the surrounding ambient is given by (Janna, 2000):

$$h_{amb} = (h_{nat}^3 + h_{for}^3)^{1/3} \tag{10}$$

where, h_{nat} and h_{for} are the natural and forced (in the case of wind) heat transfer coefficients respectively. The average Nusselt number for natural convection over the entire surface of a horizontal cylinder is given by (Churchill and Chu, 1975):

$$Nu_{nat} = \left\{ 0.6 + \frac{0.387 Ra_D^{1/6}}{\left[1 + \left(0.559 / Pr_{film} \right)^{9/16} \right]^{3/27}} \right\} \tag{11}$$

$$Ra = Gr_{L_{film}} Pr_{film} \text{ (Reyleigh number)} \quad (12)$$

$$Gr_L = \frac{g\beta_{film}(T_s - T_{amb})D_{out}^3}{\nu_{film}^2} \text{ (Grasshof number)} \quad (13)$$

$$Pr = \frac{C_{p_{film}}\mu_{film}}{\kappa_{film}} \text{ (Prandtl number)} \quad (14)$$

$$\beta_{film} = -\frac{1}{\rho_{film}} \left(\frac{\partial \rho_{film}}{\partial T_{film}} \right) \quad (15)$$

$$T_{film} = \frac{T_s + T_{amb}}{2} \quad (16)$$

where, β , D_{out} , ν and μ are the coefficient of volume expansion, the outer diameter of the pipe, the kinematic and dynamic viscosity respectively. The subscript, *film* represents the ambient air properties at the film temperature.

For forced convection, the average heat transfer coefficient over the entire surface is given by (Churchill and Bernstein, 1977):

$$Nu_{for} = 0.3 + \frac{0.62 Re_{film}^{1/2} Pr_{film}^{1/3}}{\left[1 + (0.4 / Pr_{film})^{1/4}\right]} \left[1 + \left(\frac{Re}{282000}\right)^{5/8}\right]^{4/5} \quad (17)$$

where Nu_{for} , Re_{film} and Pr_{film} are the Nusselt, Reynolds and Prandtl number at film temperature respectively.

2.2.3 Axial forced convective heat transfer between the escaping fluid and the puncture plane

The high velocity fluid escaping through the puncture is assumed to be fully developed and turbulent ($Re > 10^6$) (Mahgerefteh and Atti, 2006). As such the main mode of heat transfer will be forced turbulent convection. The corresponding Nusselt number is given by (Gnielinsky, 1976) :

$$Nu = \frac{(f_w/8)(Re-1000)Pr}{1 + 12.7(f_w/8)^{0.5}(Pr^{2/3}-1)} \quad (18)$$

Depending on the prevailing temperature and pressure, the discharging fluid may be single or two-phase. In the latter case, the heat transfer coefficient h_f is given by (Steiner and Taborek, 1992):

$$\frac{h_f}{h_l} = \left[(1-x)^{1.5} + 1.9x^{0.6} \left(\frac{\rho_l}{\rho_g} \right)^{0.35} \right]^{1.1} \quad (19)$$

where, x , ρ_g and ρ_l are the fluid quality vapour and liquid densities respectively. h_l is the heat transfer coefficient for the liquid phase, in turn given by

$$\frac{h_l D_{in}}{k_l} = 0.023 \left[\frac{\rho_{mix} u (1-x) D_{in}}{\mu_l} \right]^{0.8} \left[\frac{\mu_l C_{pl}}{k_l} \right]^{0.4} \quad (20)$$

where k_l , ρ_{mix} , u , C_{pl} , and μ_l are respectively the thermal conductivity of the liquid, the two-phase mixture density, the mixture velocity, the liquid specific heat and liquid viscosity respectively.

2.2.4 Convective heat transfer between the flowing fluid and the inner pipe wall

Depending on the puncture diameter and the flow conditions, the heat transfer between the flowing fluid and the inner pipe wall away from the puncture may be in the form of laminar or turbulent convection. For turbulent flow, equation (18) applies. For laminar flow, the Nusselt number can be determined from (Edwards et al., 1979):

$$Nu = 3.66 + \frac{0.065(D_{in}/L) Re Pr}{1 + 0.04[(D_{in}/L) Re Pr]^{2/3}} \quad (21)$$

where L is the pipe length.

2.3 Fracture Mechanics

The quasi-adiabatic expansion of the escaping fluid will result in the cooling of the pipe wall in the proximity of the puncture. If the temperature at the crack tip falls below the pipeline material DBTT, depending on the prevailing thermal and pressure stresses, the material may fail in a brittle manner, in which case linear-elastic fracture mechanics becomes applicable. As such, the mode 1 stress intensity factor, K_I , is used as the fracture parameter in this study (Pook, 2000; Westergaard, 1939).

In the absence of an analytical solution for a non-uniform defect geometry considered in this study, the weight function method (Rice, 1972) is used to evaluate the K_I at the crack tip.

The weight function at any distance, x along the crack length a , is given by:

$$h(x,a) = \frac{H}{2K_I} \frac{\partial u_r(x,a)}{\partial a} \quad (22)$$

where for plane stress, $H = E$ and for plane strain, $H = \frac{E}{1-\nu^2}$. E , ν and $u_r(x,a)$ are the Young's modulus, Poisson's ratio and crack displacement respectively.

Using equation (22), the stress intensity factor, K_I , can be expressed as

$$K_I = \int_{\Gamma_c} \sigma(x) h(x,a) dx \quad (23)$$

where $\sigma(x)$ and Γ_c are the stress distribution along the crack face in the uncracked geometry and the perimeter of the crack respectively.

Following Brennen (1994), the weight function can be expressed in the form of a power series given as:

$$h(x,a) = \frac{H}{2K_I(a)} \frac{\partial u(x,a)}{\partial a} = \frac{2\sigma_0}{HK_I(a)} \sqrt{2} \sum_{j=0}^m C_j \left(1 - \frac{x}{a}\right)^{j-1/2} \quad (m \geq 2) \quad (24)$$

$$C_0 = \frac{F\left(\frac{a}{L}\right)}{2} \quad F\left(\frac{a}{L}\right) = \frac{K_r}{\sigma_0 \sqrt{\pi a}} \quad (25)$$

where C_j are unknown coefficients to be determined which depend on the defect geometry only. m , on the other hand is the number of symmetrical reference loading stresses.

The coefficients C_j can be found from at least two reference stress intensity factor solutions with corresponding reference stress loading. Considering the situation where two reference cases are available:

$$C_1 = \frac{q_1 W_{22} - q_2 W_{12}}{W_{11} W_{22} - W_{21} W_{12}} \quad (26)$$

$$C_2 = \frac{q_2 W_{11} - q_1 W_{21}}{W_{11} W_{22} - W_{21} W_{12}} \quad (27)$$

where q_i and W_{ij} are defined as:

$$W_{ij} = \int_0^a \sigma_i(x) \sum_{j=0}^m \left(1 - \frac{x}{a}\right)^{j-1/2} dx \quad (28)$$

$$q_i = \frac{F_1\left(\frac{a}{L}\right)}{2} \left[K_i(a) \sqrt{\frac{\pi a}{2} - W_{i0}} \right] \quad (29)$$

where $K_i(a)$ is the stress intensity factor of i^{th} loading case.

For a given defect geometry, the above method requires at least two stress intensity factor solutions under independent stress loadings to develop the weight function. The finite element method using the commercially available software, ABAQUS (SIMULIA, 2011) is employed for this purpose. Here, the pipeline is modelled as cylindrical tube of defined diameter and thickness, incorporating a puncture of a given geometry on its wall.

3. Results and Discussion

The following describes the results of the application of the brittle fracture described above to a 10 km long, 609.6 mm o.d. hypothetical gas or dense phase CO₂ pipeline made of British Gas LX/1 steel. The fracture toughness values above and below the Ductile-Brittle-Transition Temperature (DBTT) are taken as 95 MPa m^{0.5} and 40 MPa m^{0.5} respectively. These values are assumed constant at any temperature away from the DBTT.

The two pipeline failure scenarios considered are as follows:

- 1) above ground exposed pipeline (no insulation);
- 2) buried pipeline.

As part of the analysis, the pipe wall thickness, DBTT and defect shape are varied in order to investigate their impact on the fracture propagation behaviour. The examined flow conditions include isolated (i.e. no flow within the pipeline prior to failure) and unisolated flows where pumping continues despite rupture.

Unless otherwise stated, the initial through wall defect shape is assumed to be a 20 mm dia. circular puncture with a 20-mm hairline fracture extending from its side, running parallel to the main pipeline axis. The inventory is assumed to be pure CO₂. Table 1 presents the prevailing conditions for the simulation tests conducted.

Inventory	100% CO ₂
Feed pressure (bara)	34 (gas phase), 150 (dense phase)
Ambient and feed temperature (K)	283.15
Overall pipeline length (km)	10
Pipeline wall thickness (mm)	5, 6, 9, 14.7
Pipeline external diameter (mm)	609.6
Failure mode	puncture
Puncture diameter (mm)	20
Equation of state	Modified Peng Robinson
Pipe material	British Gas LX/1
Pipe roughness (mm)	0.05
Pipe wall thermal conductivity (W/(m·K))	53.65
Pipe wall heat capacity (J/(kg·K))	434
Feed flow rate (m/s)	0, 0.2 m/s
DBTT (°C)	0, -10
K _{Ic} (MPa m ^{0.5})	95 (ductile), 40 (brittle)

Table 1 Pipeline Characteristics and prevailing condition for the test cases

3.1 Crack Propagation in Exposed Pipelines

In the case of the exposed pipeline, the simulations are conducted for both gas and dense phase CO₂ transportation. CO₂ is considered to be in the dense phase when above its critical pressure (73.8 bara) and below its critical temperature (31.1 °C). To satisfy the 50% Specified Minimum Yield Strength requirement for the operating pressures (see table 1), the respective pipe wall thicknesses for each case are calculated as 6 mm (gas phase) and 14.7 mm (dense phase) respectively. The pipeline material is assumed to comply with British Gas LX/1 specification corresponding to a DBTT of 0 °C. In both cases, the pipeline is assumed to be isolated upon failure.

Figure 1 shows the transient axial pipe temperature profiles at different time intervals in the proximity of the puncture plane for gas phase CO₂ at 10 °C. The rapid expansion of the escaping inventory results in significant cooling of the pipe wall with the effect becoming more pronounced with time and distance towards the puncture plane. According to the data, the pipe wall temperature at ca. 7 cm either side of the puncture reaches the DBTT of 0 °C in less than 60 s following puncture, dropping to a minimum temperature of -23 °C at its centre.

Figure 2 shows the corresponding variation of the crack length against time following the puncture. According to the data, the crack begins to grow upon puncture, reaching a maximum length of ca. 70 mm at 1000 s following rupture, becoming unstable beyond this point leading to catastrophic pipeline failure.

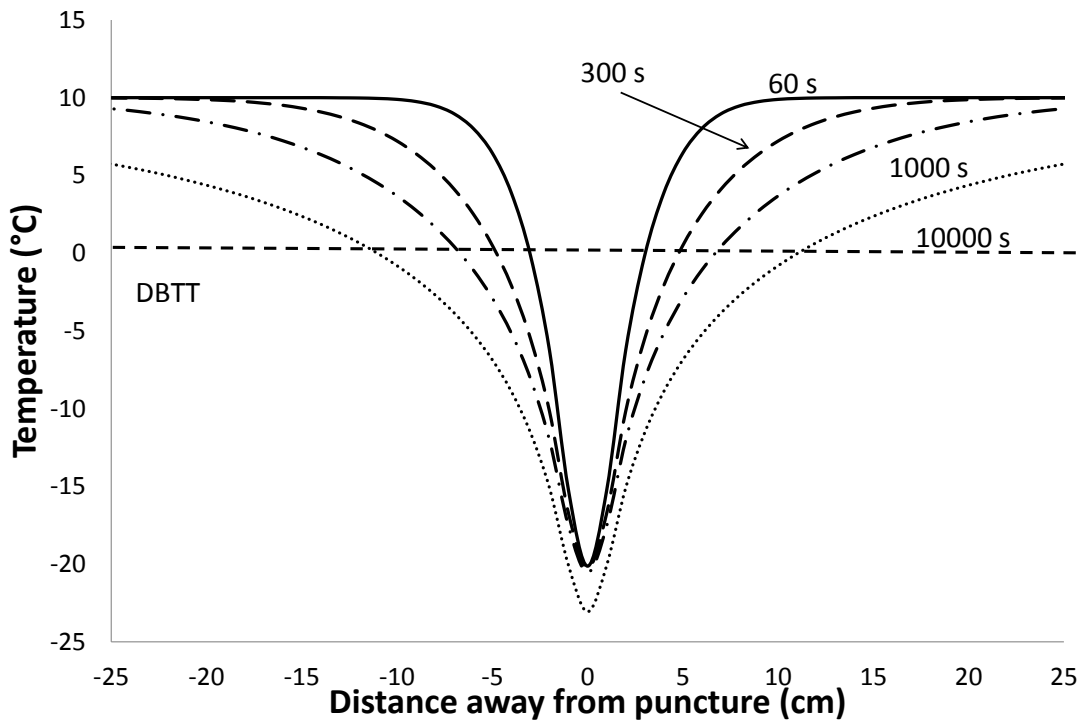


Figure 1. The variation of the pipe wall temperature in the proximity of the puncture with time for gas phase CO₂ (34 bara, 10 °C; exposed pipeline)

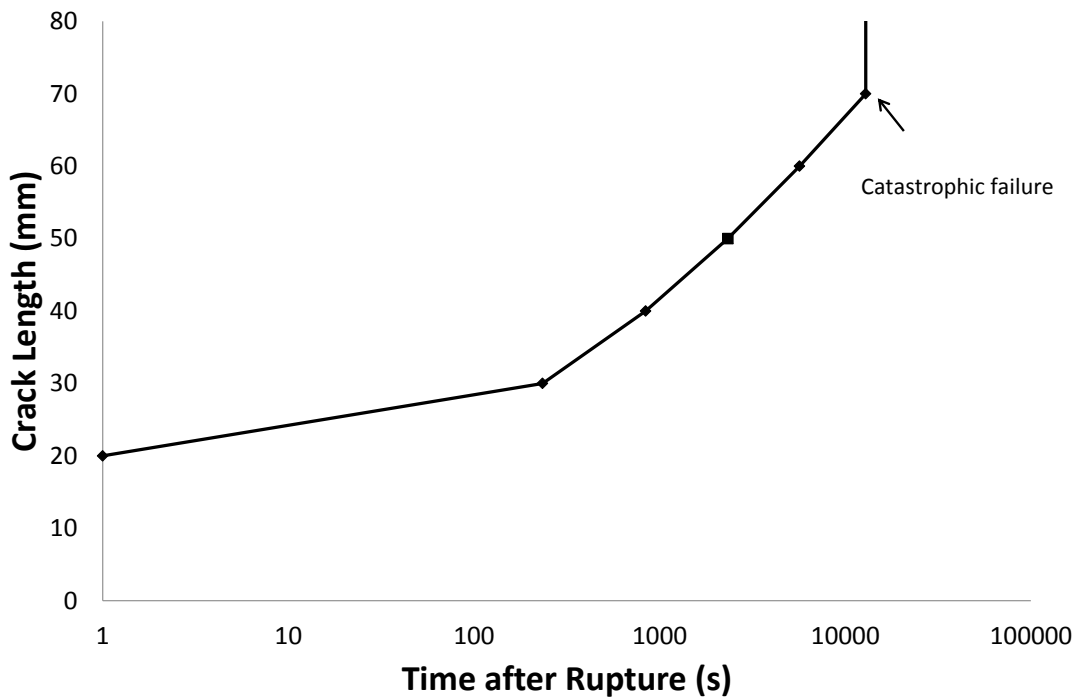


Figure 2. Variation of the crack length against time following the puncture of the gas phase CO₂ pipeline (34 bara, 10 °C; exposed pipeline).

Figures 3 and 4 respectively show the same data as in figures 1 and 2, but this time for a pipeline containing dense phase CO₂ at 150 bara. It is clear from figure 3 that the minimum temperature at the defect centre reaches to only -2 °C (c.f. -23 °C for gas phase CO₂). The initial crack tip temperature 20 mm away from the puncture always stays above the DBTT. Hence, for the conditions tested, crack propagation will not occur in the exposed pipeline containing dense phase CO₂.

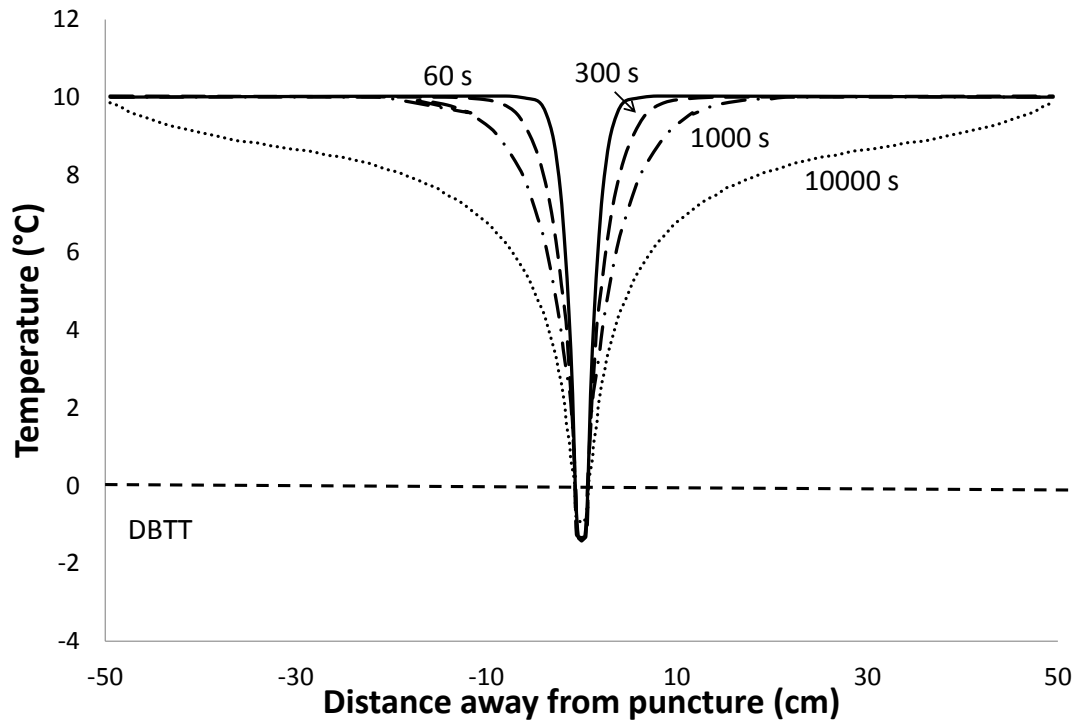


Figure 3. The variation of the pipe wall temperature in the proximity of the puncture with time for dense phase CO₂ (150 bara, 10 °C, exposed pipeline)

3.2 Crack Propagation in Buried Pipelines

In the following simulations, all of the pipeline characteristics and the prevailing conditions are taken to be the same as those given table 1 with the exception that the pipeline is assumed to be buried. The backfill soil is taken to be sand with thermal conductivity and mean particle size of 0.95 W/mK and 1.35 mm respectively. Furthermore, it is assumed that there is no blowout of the surrounding soil following the initial puncture given its small diameter. The simulations are performed for gas and dense phase CO₂ inventories..

Figure 4 shows the transient pipe wall temperature in the proximity of the puncture at different time intervals up to 10,000 s following puncture for the pipeline transporting gas phase CO₂ (34 bar and 10 °C). Figure 5 shows the same data as in figure 4 but for the dense phase CO₂ (150 bar and 10°C). In both cases, the pipeline is assumed to be isolated upon failure corresponding to zero feed flow.

Returning to figure 4 for the gas phase CO₂ pipeline, the following observations may be made:

- i) the minimum pipe wall temperature at the puncture location remains at - 20 °C for the entire duration of the release period of 10, 000 s under consideration;
- ii) in the first 1,000 s following puncture, the minimum pipe wall temperature corresponds to the release location. Also, the pipe wall temperature away from the puncture plane decreases with the passage of time;
- iii) at around 5,000 s, a switchover takes place where the pipe wall temperature away from the puncture plane drops below that at the puncture plane, falling to a minimum temperature of -55 °C at ca 1,000 s. This switchover is due to the eventual secondary cooling of the pipe wall by the surrounding soil cooled by the low temperature (ca. -70 °C) escaping CO₂.

Similar trends in the data may be observed for dense phase CO₂ (figure 5) with the exception that the minimum rupture plane temperature before the switch over takes place is -2 °C (c.f -20 °C for gas phase; see figure 5). On the other hand the minimum temperature away from the puncture plane at 10,000 s following puncture is ca – 42 °C (c.f – 55 °C for gas phase CO₂: figure 4).

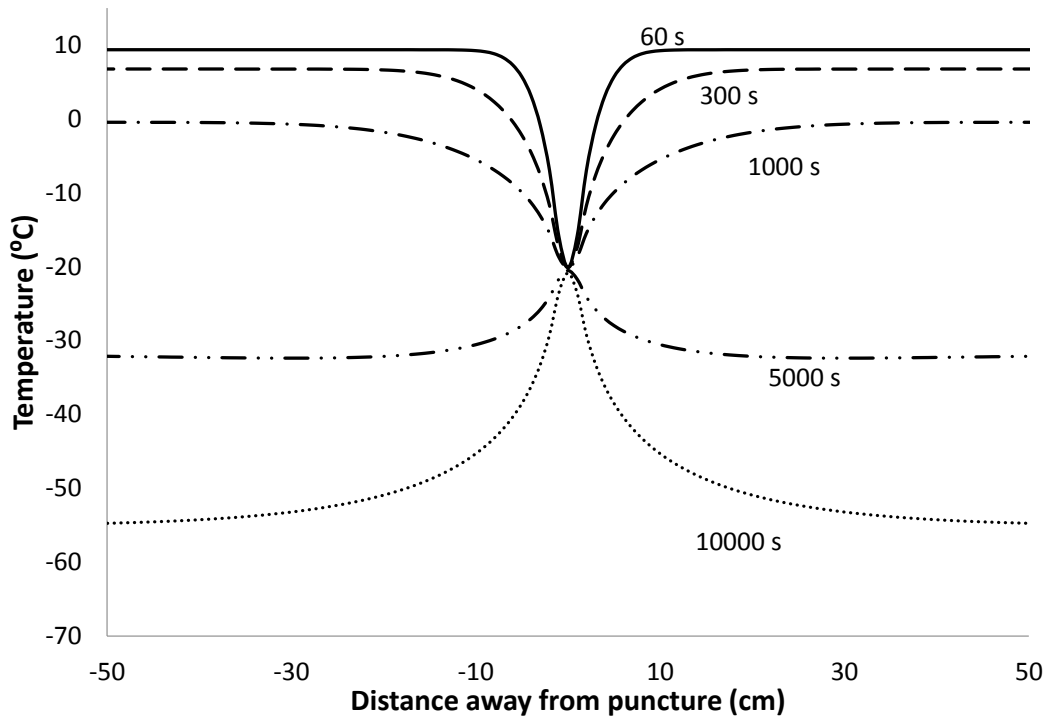


Figure 4. The variation of the pipe wall temperature in the proximity of the puncture with time for the gas phase CO₂ pipeline (34 bara, 10 °C; buried pipeline, no soil blow out)

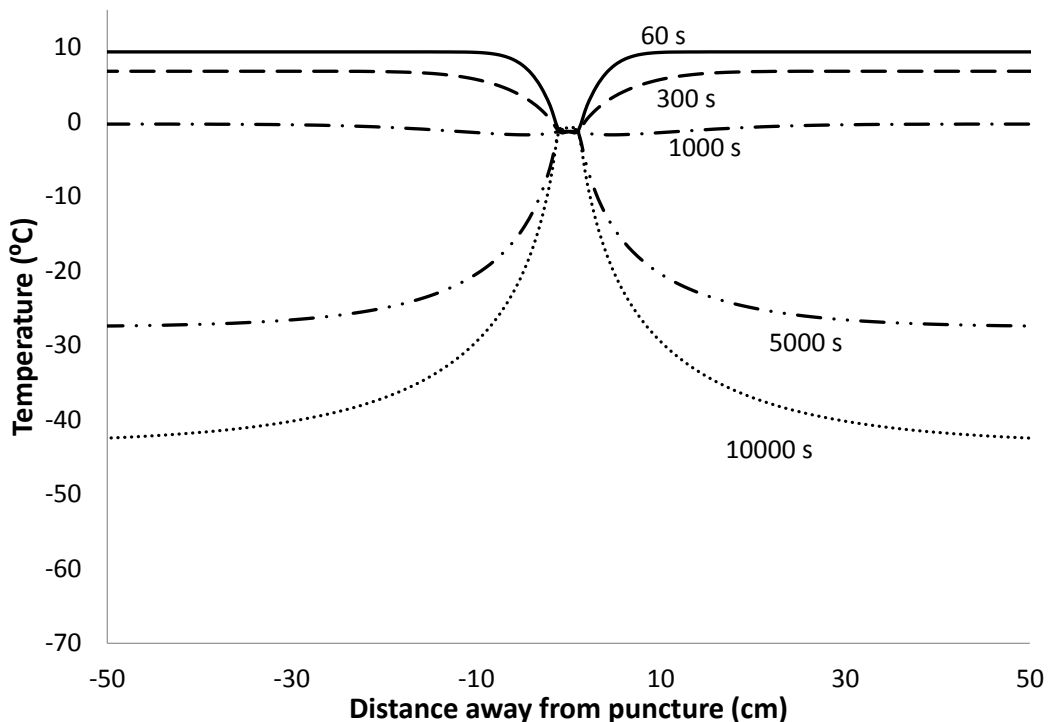


Figure 5. The variation of the pipe wall temperature in the proximity of the puncture with time for the dense phase CO₂ pipeline (150 bara; 10 °C, buried pipeline, no soil blow out)

Figure 6 shows the corresponding variation of the crack length against time following the puncture of the buried pipeline transporting gas and dense phase CO₂. As it may

be observed, for the gas phase buried pipeline, it only takes 360 s following the initial puncture for the crack to become unstable. This compares to ca. 1,000 s for the exposed pipeline (see figure 2). The considerably shorter time span needed to reach unstable crack in the former case is due to the secondary cooling of the pipe wall by the surrounding soil exposed to the escaping low temperature CO₂. The same process is also responsible for promoting crack propagation in the dense phase CO₂ pipeline, where the crack starts becomes unstable ca.774 s following puncture. As it may be recalled, no crack propagation was observed in the case of the exposed pipeline transporting dense phase CO₂ (see figure 4).

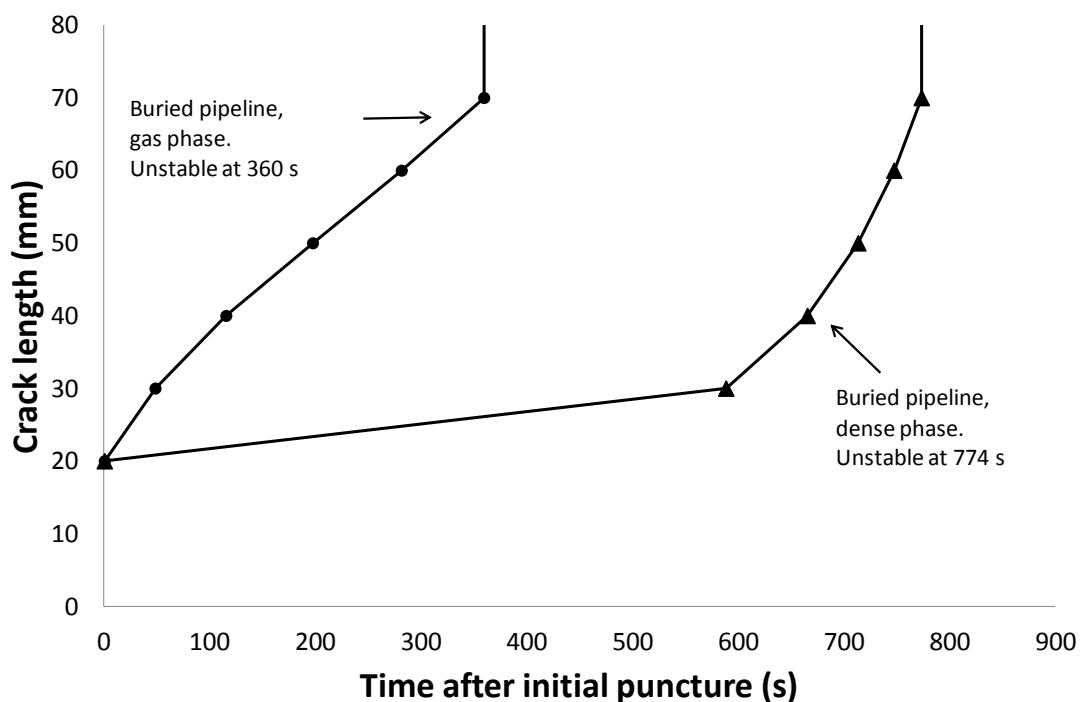


Figure 6. Variation of the crack length against time following the puncture for pipeline transporting gas and dense phase CO₂ (34 bara and 150 bara; 10 °C, buried pipeline, no soil blow out).

3.3 Sensitivity Analysis

3.3.1 Impact of Pipe Wall Thickness

Figure 8 shows the impact of the pipe wall thicknesses (5, 6 and 9 mm) on the crack propagation behaviour against time for the exposed gas phase CO₂ pipeline. The results for the 6 mm wall thickness are the same as those presented in figure 2, where

the crack became unstable at ca. 1,000 s following puncture. As it may be observed, decreasing the pipe wall thickness to 5 mm, results in the much earlier catastrophic failure at ca. 320 s following puncture.

Increasing the pipe wall thickness to 9 mm on the other hand results in no crack propagation despite the fact that crack tip temperature drops below the DBTT (see figure 1).

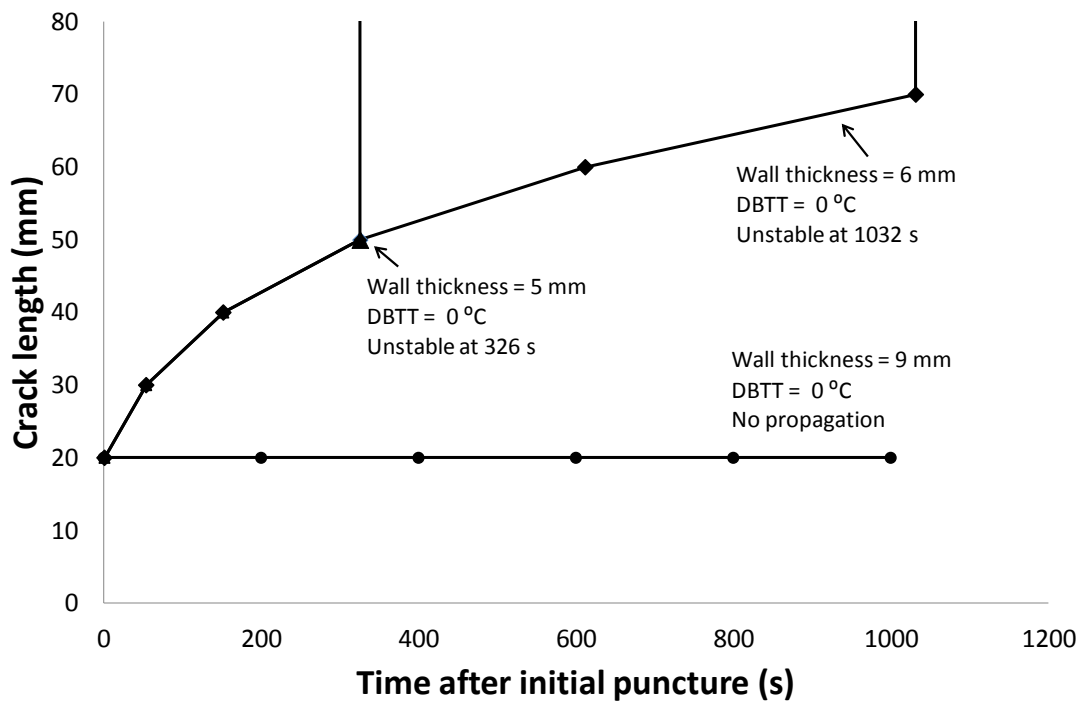


Figure 7. Comparison of the variation of the crack length against time after puncture with various pipe wall thicknesses; exposed pipeline, gas phase CO₂

3.3.2 Impact of Ductile-Brittle-Transition Temperature

Figure 8 shows the effect of varying the DBTT of the pipe material on the crack propagation behaviour following puncture for the gas phase CO₂ pipeline (see table 1). As it may be observed, when the DBTT is 0 °C, it takes 326 s and 1036 s for the cracks to reach the critical condition for the 5 mm and 6 mm pipe wall thicknesses respectively. However, reducing the pipe wall material DBTT to -10 °C has a dramatic impact on the fracture propagation behaviour. For both pipe wall thicknesses, the initial crack grows by only 10 mm, coming to rest at ca. 2,900 s after the initial

puncture. Noting that modern pipeline steels normally have a DBTT of $-70\text{ }^{\circ}\text{C}$, it is highly unlikely that the brittle fracture will occur in a gas phase exposed CO_2 pipeline.

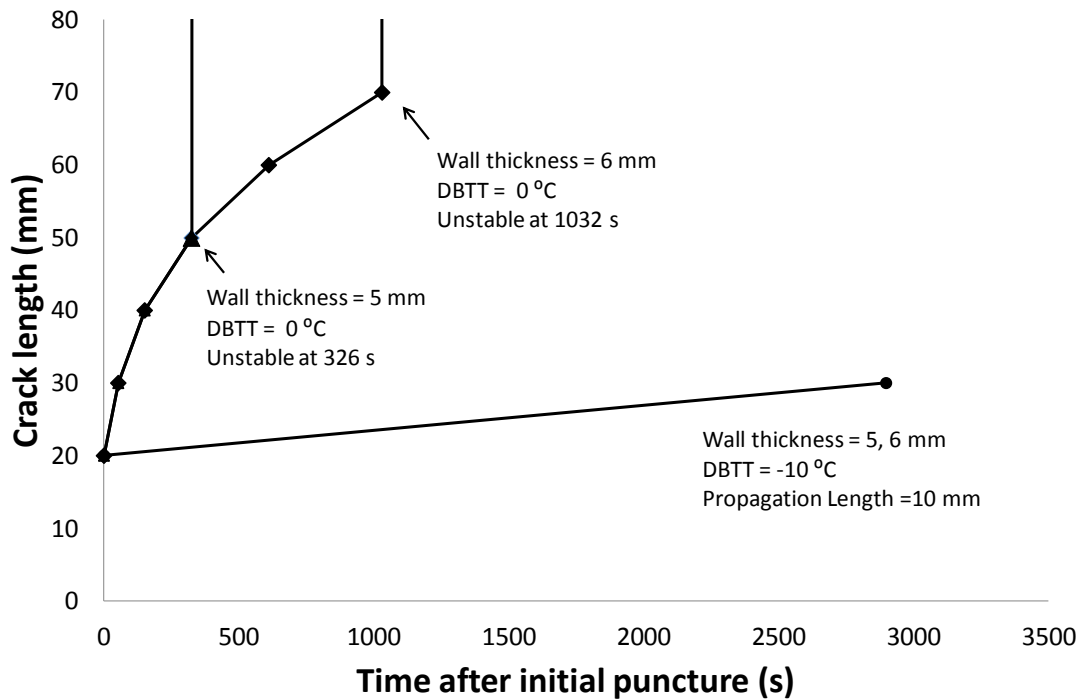


Figure 8. Comparison of the variation of the crack length against time following the puncture with various DBTT; exposed pipeline, gas phase CO_2 .

3.3.3 Impact of Feed Flow

Figure 9 shows the fracture propagation behaviour for the gas phase CO_2 pipeline (DBTT = $0\text{ }^{\circ}\text{C}$ and pipe thickness of 6 mm; table 1), for both isolated and unisolated flows, exposed pipeline. In the latter case, the feed flow into the pipe is assumed to remain at 0.2 m/s throughout the decompression process. As it may be observed, in the case of unisolated flow, the crack arrests after 247 s following puncture. This compares to unstable crack propagation at 1,032 s following puncture for the isolated pipeline. Remarkably and counter-intuitively, the above observation means that for the case examined, emergency isolation of the flow following the formation of the initial defect results in unstable fracture propagation.

The above observation may be explained by reference to figure 10 showing the corresponding variation of the pipe wall temperature profile in the proximity of the

puncture at two time intervals of 300 s and 5,000 s following puncture for both the isolated and unisolated flow scenarios. As it may be observed, at 300 s, both the isolated and unisolated flow scenarios show similar temperature profiles. However, at 5,000 s following the initial puncture, the feed flow in the unisolated pipeline results in a lower degree of cooling of the pipe wall as compared to the isolated case (cf -18 °C with -23 °C). This indicates that the relatively warm (10 °C) bulk fluid flowing within the pipe reduces the amount of localised cooling of the pipe wall, thus increasing its resistance to brittle fracture propagation.

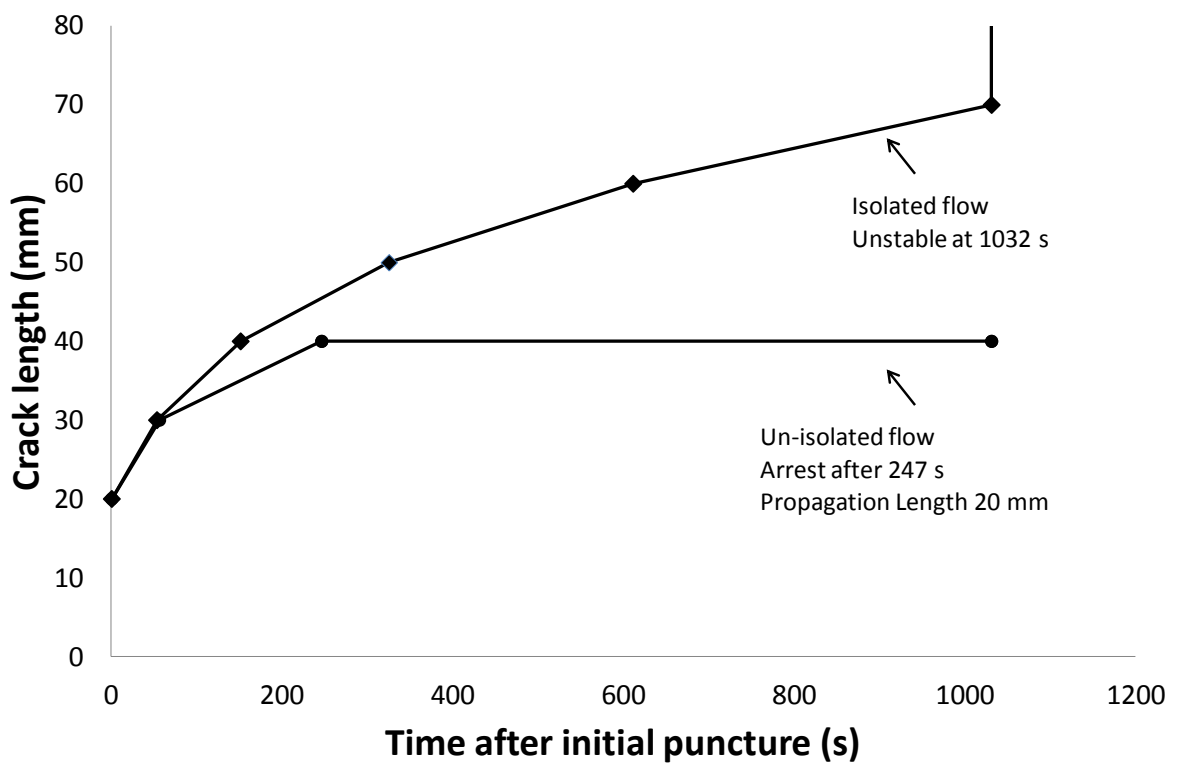


Figure 9. Variation of the crack length against time following the puncture of the gas phase pipeline for isolated and unisolated flows.

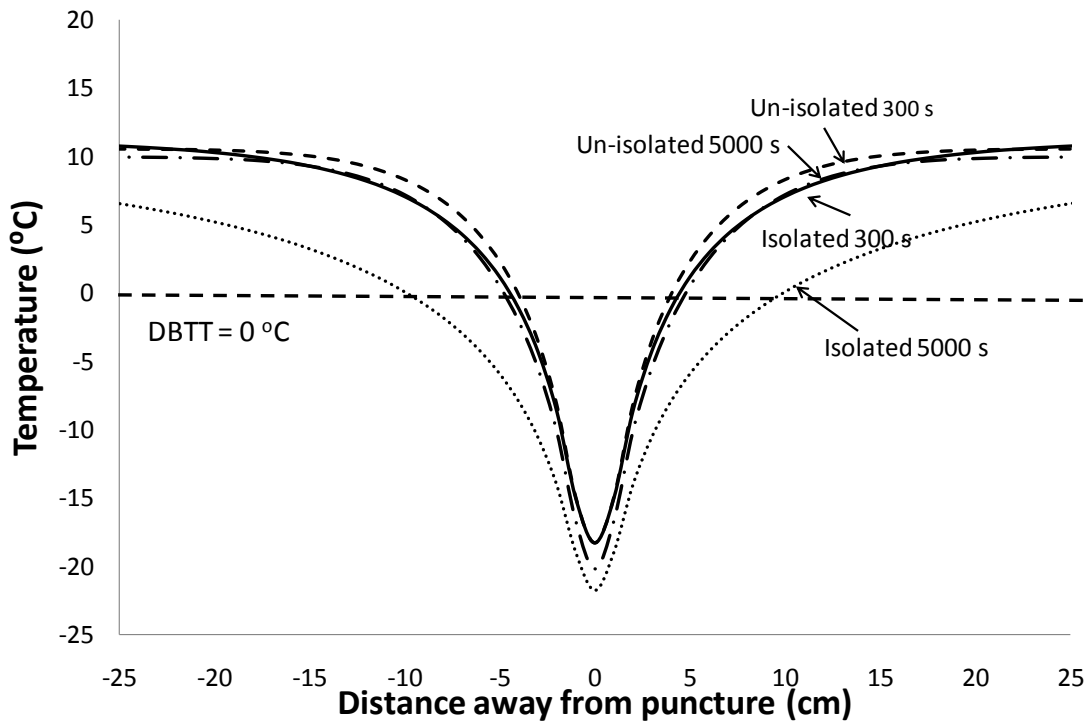


Figure 11. Comparison of pipe wall temperature profiles 300 s and 5,000 s following puncture of the gas phase pipeline for isolated and unisolated flows

3.3.4 Impact of Stream Impurities

Figure 12 shows the impact of stream impurities in the dense phase CO₂ stream (150 bar and 10°C) on the variation of the pipe wall temperature in the proximity of the puncture at 10,000 s following the initial puncture. The corresponding composition of CO₂ mixtures examined represent those based on post-combustion and pre-combustion (Cosham et al., 2011) capture technologies are given in table 2. Given the established significant impact of the presence N₂ in promoting ductile failures (Mahgerefteh et al., 2012) the data also include two hypothetical mixtures of CO₂ and N₂ (5% v/v and 10%) representing extreme cases.

Returning to figure 12, as it may be observed, within the ranges tested, impurities have negligible impact on the resulting pipe wall temperature profile and hence the fracture propagation behaviour during the depressurisation process.

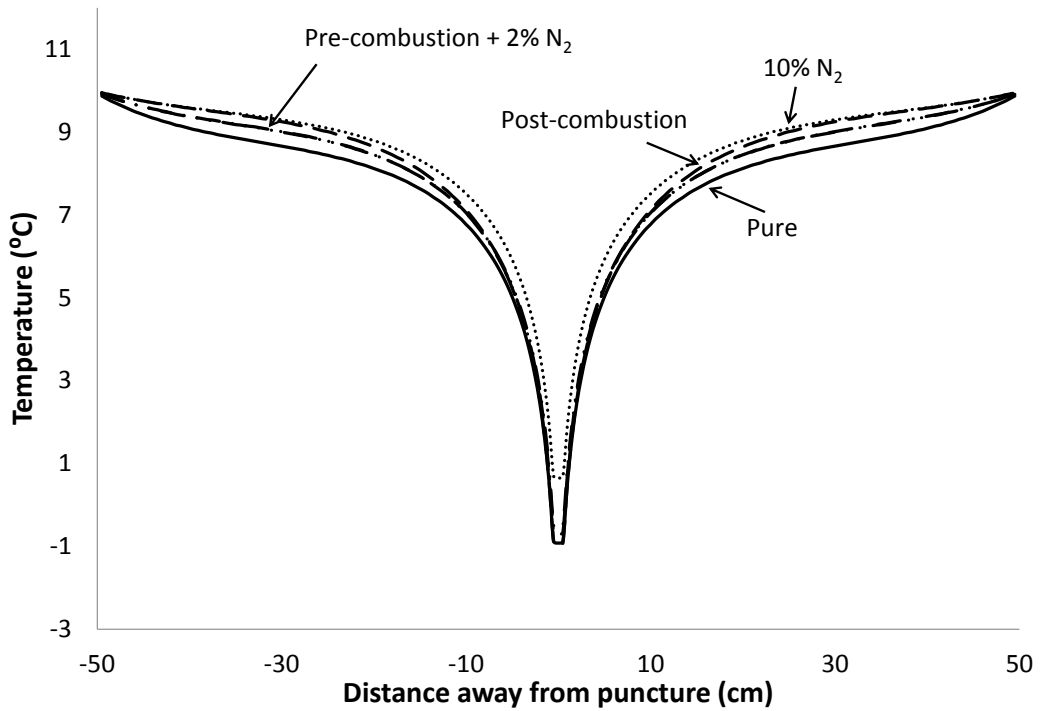


Figure 12. The impact of CO₂ composition on the pipe wall temperature profile in the proximity of the puncture plane at 10,000 s following puncture for dense phase CO₂.

	Composition (v/v)
Pure CO ₂	100% CO ₂
Pre-Combustion mixture	95.6% CO ₂ , 0.4% CO, 0.6% N ₂ , 3.4% H ₂ S
Post-Combustion mixture	99.82% CO ₂ , 0.17% N ₂ , 0.01% O ₂
CO ₂ -N ₂	95% CO ₂ , 5% N ₂
CO ₂ -N ₂	90% CO ₂ , 10% N ₂

Table 2. The % v/v composition of the various CO₂ streams assumed for the fracture propagation simulations to investigate the impact of impurities

3.3.5 Impact of Defect Shape and Size

Table 3 shows schematic representations and the characteristic dimensions represented by the symbols a, b, and c for four puncture geometries considered in order to investigate the impact of the defect shape on the fracture propagation behaviour. These include circular and elliptical punctures with hairline fractures of finite equal lengths ($a = 20$ mm) extending from either one or both sides. Such through-wall defects may form, for example, as a result of damage by a mechanical digger.

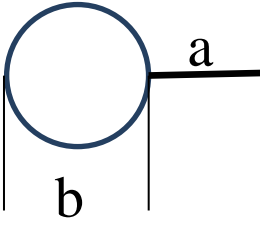
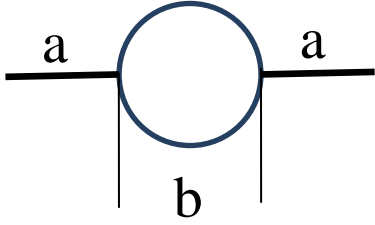
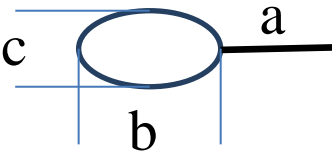
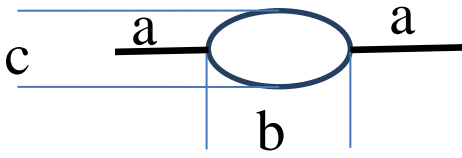
Type 1	Type 2
	
Type 3	Type 4
	

Table 3. Various puncture geometries examined for fracture analysis indicating the characteristic dimensions, a, b and c

Table 4 shows brittle fracture data for Type 1 defect geometry for different pipe wall thicknesses of 3.5, 4, 5 and 9 mm for the gas phase CO₂. Two puncture diameters of 10 and 20 mm are considered in order to investigate the impact of the defect size. The higher DBTT value of 0 °C is assumed to represent the worst-case scenario.

As it may be observed, the larger initial puncture diameter (20 mm) results in a significant reduction in the pipeline's resistance to fracture. For all but the largest pipe wall thicknesses (9 mm), uncontrolled propagating fractures would be expected.

Table 5 shows the corresponding fracture data as in table 6.3 but for type 1 to type 4 defect shapes (see table 4). For consistency, an open defect area of 3.14 cm²

equivalent to a 20 mm dia. circular hole is assumed in all cases. Based on the data presented, it is clear that the initial defect geometry has a profound impact on the pipeline's resistance to brittle fracture. The elliptical defect geometries (Types 3 and 4) are worse than the circular defect geometries. Also, the presence of two initial cracks on either side of the defect dramatically reduces the pipe wall's resistance to brittle fracture propagation.

Wall thickness (mm)	Puncture diameter = 20 mm		Puncture diameter = 10 mm	
	Crack state	Time(s)	Crack state	Time(s)
3.5	Unstable	Instant	Unstable	2,458
4	Unstable	234	Unstable	24,632
5	Unstable	2,330	Arrest, 40 mm	25,300
9	No growth	-	No growth	-

Table 4. Gas phase brittle fracture propagation behaviour for Type 1 defect geometry

Wall thickness (mm)	Type 2		Type 3		Type 4	
	Crack state	Time(s)	Crack state	Time(s)	Crack state	Time(s)
3.5	Unstable	Instant	Unstable	Instant	Unstable	Instant
4	Unstable	40	Unstable	40	Unstable	Instant
5	Unstable	234	Unstable	2,330	Unstable	40
9	No growth	-	Arrest, 40 mm	43,818	Arrest, 40 mm	43,818

Table 5. Gas phase brittle fracture propagation behaviour for Types 2–4 defect geometries (defect area = 3.14 cm²)

4. Conclusion

It is widely accepted that pressurised pipelines will present the main method for transporting captured CO₂ from fossil fuel power plants and other CO₂ intensive industries for subsequent sequestration. Given the CO₂ is an asphyxiant at high

concentrations, the safety of such pipelines in the unlikely event of pipeline failure is of fundamental importance.

The relatively high Joule-Thomson expansion cooling of CO₂, coupled with its slow depressurisation, raises concern that a situation may arise in which a seemingly inconsequential small diameter through wall defect may eventually transform into a catastrophic running brittle fracture.

So far most of the studies on this topic have focused on predicting the minimum pipe wall temperature and comparing it with the pipe wall material ductile to brittle transition temperature. In the absence of knowledge of the accompanying pressure and temperature stresses in the pipe wall, this information on its own is not enough to determine if and when the initial leak in the pipe wall will transform into a propagating fracture.

In this paper, a rigorous fluid/structure interaction model for simulating the above process is presented. The model accounts for all the important processes governing the fracture propagation process including fluid/wall heat transfer effects, the resulting localised thermal and pressure stresses in the pipe wall as well as the initial defect geometry. Real fluid behaviour is considered using the modified Peng Robinson equation of state for CO₂.

The application of the fracture model to hypothetical but realistic failure scenarios using British Gas LX/1 pipeline materials reveals significant, and to some extent, unexpected findings. For example:

- gas phase CO₂ pipelines are more susceptible to undergoing a propagating brittle fracture as compared to dense phase CO₂ pipelines, despite the lower operating pressures in the former case. This is shown to be primarily a consequence of the higher Joule Thomson expansion induced cooling of gaseous CO₂.

- a buried CO₂ pipeline is more susceptible to brittle fracture propagation as compared to an above ground pipeline due to the eventual secondary cooling of the pipe wall by the surrounding soil in contact with it.
- isolation of the feed flow to the pipeline following a leak promotes brittle fracture propagation.
- an increase in the pipe wall thickness dramatically increases the pipeline's resistance to brittle fracture failure.
- the initial through wall defect geometry in the pipeline has a profound impact on the pipeline's propensity to brittle fracture failure. A fracture may only propagate provided the initial through wall defect incorporates a sharp edge where the stress concentration may be large enough to drive a crack.
- within the ranges tested, CO₂ stream impurities representative of the main capture technologies do not have an appreciable impact on the pipeline's resistance in undergoing brittle fracture failure.

Finally, it should be noted that in contrast to ductile failures, brittle fracture propagation is a time dependent phenomenon. It will only occur if the depressurization duration is sufficiently long such that at the time when the pipe wall temperature in the vicinity of the defect drops below the DBTT, the accompanying thermal and pressure stresses exceed the pipe wall fracture toughness.

Acknowledgments

The work has been conducted under the auspices of the MATTRAN project (Materials for Next Generation CO₂ Transport Systems) and the authors gratefully acknowledge the financial support of EPSRC and E.ON for this research (E.ON-EPSRC Grant Reference EP/G061955/1).

References

- Andrews, R., Haswell, J., Cooper, R., 2010. Will fractures propagate in a leaking CO₂ pipeline? *Journal of Pipeline Engineering* 9, 277 – 287
- API, 2009. ANSI/API Specification 5L Specification for Line Pipe. American Petroleum Institute.
- Bendiksen, K.H., Malnes, D., Moe, R., Nuland, S., 1991. The dynamic two-fluid model OLGA: theory and applications. *SPE Production Eng* 6, 171.
- Bilio, M., Brown, S., Fairweather, M., Mahgerefteh, H., 2009. CO₂ pipelines material and safety considerations, IChemE Symposium Series: HAZARDS XXI Process Safety and Environmental Protection. 423 – 429.
- Bisgaard, C., Sorensen, H.H., 1987. A finite element method for transient compressible flow in pipelines. *International Journal for Numerical Methods in Fluids* 7, 291 – 303.
- Brennan, F., 1994. Evaluation of stress intensity factors by multiple reference state weight function approach. *Theoretical and Applied Fracture Mechanics* 20, 249–256.
- Cengel, Y.A., 2003. *Heat Transfer: A Practical Approach*, second ed. McGraw-Hill Higher Education.
- Chen, J. R., Richardson, S.M., Saville, G., 1995. Modelling of Two-Phase Blowdown from Pipelines – I. A hyperbolic model based on variational principles. *Chemical Engineering Science*. 50, 695 – 713
- Chen, J. R., Richardson, S. M., Saville, G., 1995. Modelling of Two-Phase Blowdown from Pipelines - II. A simplified numerical method for method for multi-component mixtures. *Chemical Engineering Science* 50, 2173–2187.
- Chen, N.H., 1979. An explicit equation for friction factor in pipes. *Industrial and Engineering Chemistry Fundamentals*. 18, 296–297.
- Churchill, S.W., Bernstein, M., 1977. A Correlating Equation for Forced Convection from Gases and Liquids to a Circular Cylinder in Cross Flow. *Journal of Heat Transfer* 99, 300–306.
- Churchill, S.W., Chu, H.H.S., 1975. Correlating Equations for Laminar and Turbulent Free Convection from a Horizontal Cylinder. *International Journal of Heat Mass Transfer* 18, 1049–1053.
- Cosham, A., Eiber, R.J., 2008. Fracture Control in Carbon Dioxide Pipelines: The Effect of Impurities, 7th International Pipeline Conference (IPC2008). Calgary, 229 – 240.

- Edwards, D.K., Denny, V.E., Mills, A.F., 1979. *Transfer Processes*. Washington, DC: Hemisphere.
- Eftring, B., 1990. Numerisk beräkning av temperaturförlopp. Numerical calculations of thermal processes. The Swedish Council for Building Research, Report R81:1990.
- Gnielinsky, V., 1976. New Equations for Heat and Mass Transfer in Turbulent Pipe and Channel Flow. *International Journal of Chemical Engineering* 16, 359-368.
- Harper, P., Wilday, J., Bilio, M., 2011. Assessment of the major hazard potential of carbon dioxide (CO₂). Health and Safety Executive.
- Janna, W.S., 2000. *Engineering Heat Transfer*. CRC Press.
- Mahgerefteh, H., Atti, O., 2006. Modeling low-temperature-induced failure of pressurized pipelines. *AIChE Journal* 52, 1248–1256.
- Mahgerefteh, H., Brown, S., Denton, G., 2012. Modelling the impact of stream impurities on ductile fractures in CO₂ pipelines. *Chemical Engineering Science* 74, 200–210.
- Mahgerefteh, H., Brown, S., Zhang, P., 2011. A dynamic boundary ductile-fracture-propagation model for CO₂ pipelines. *Journal of Pipeline Engineering* 9, 265–276.
- Mahgerefteh, H., Denton, G., Rykov, Y., 2008. A hybrid multiphase flow model. *AIChE Journal* 54, 2261–2268.
- Mahgerefteh, H., Rykov, Y., Denton, G., 2009. Courant, Friedrichs and Lewy (CFL) impact on numerical convergence of highly transient flows. *Chemical Engineering Science* 64, 4969–4975.
- Maxey, W.A., 1974. *Fracture Initiation, Propagation and arrest*. Battelle Memorial Institute. Columbus Laboratories.
- Oke, A., Mahgerefteh, H., Economou, I., Rykov, Y., 2003. A transient outflow model for pipeline puncture. *Chemical Engineering Science* 58, 4591–4604.
- Parfomak, P.W., Fogler, P., 2007. *Carbon Dioxide (CO₂) Pipelines for Carbon Sequestration: Emerging Policy Issues*. Congressional Research Service: Washington, DC.
- Pook, L.P., 2000. *Linear Elastic Fracture Mechanics for Engineers: Theory and Applications*. WIT Press.
- Rice, J.R., 1972. Some Remarks on Elastic Crack-Tip Stress Fields. *International Journal of Solids and Structures* 8, 751–758.
- Seevam, P.N., Race, J.M., Downie, M.J., Hopkins, P., 2008. Transporting the next generation of CO₂ for carbon capture and storage: the impact of impurities on supercritical CO₂ pipelines, 7th International Pipeline Conference, Calgary. 39–51.

Serpa, J., Morbee, J., Tzimas, E., 2011. Technical and Economic Characteristics of a CO₂ Transmission Pipeline Infrastructure. JRC Scientific and Technical Reports. European Commission Joint Research Centre Institute for Energy. 51.

SIMULIA, 2011. ABAQUS FEA, Dassault Systèmes

Steiner, D., Taborek, J., 1992. Flow boiling heat transfer in vertical tubes correlated by an asymptotic method. Heat Transfer Engineering 13. 43-69

Suehiro, Y.; Nakajima, M.; Yamada, K.; Uematsu, M., 1996, Critical parameters of {xCO₂ + (1 - x)CHF₃} for x = (1.0000, 0.7496, 0.5013 , and 0.2522), The Journal of Chemical Thermodynamics 28, 1153-1164.

Tannehill, J.C., Anderson, D.D.A., Pletcher, R.H., 1997. Computational fluid mechanics and heat transfer. Taylor & Francis.

Westergaard, H.M., 1939. Bearing Pressures and Cracks. Journal of Applied Mechanics 6, 49-53

Wu, D., Chen, S., 1997. A Modified Peng-Robinson Equation of State. Chemical Engineering Communications 156, 215–225.

Zucrow, M.J., Hoffman, J.D., 1975. Gas Dynamics, Volume 1 edition. Wiley. New York